crystals

MDPI

Article

Theoretical Study of Pressure-Induced Phase Transitions in Sb_2S_3, Bi_2S_3, and Sb_2Se_3

Estelina Lora da Silva [1,†,*], Mario C. Santos [2,3,†], Plácida Rodríguez-Hernández [4,†], Alfonso Muñoz [4,†] and Francisco Javier Manjón [3,†]

1 IFIMUP, Institute of Physics for Advanced Materials, Nanotechnology and Photonics, Department of Physics and Astronomy, Faculty of Sciences, University of Porto, Rua do Campo Alegre, 687, 4169-007 Porto, Portugal
2 Instituto dos Pupilos do Exército, Estrada de Benfica, nº 374, 1549-016 Lisboa, Portugal
3 Instituto de Diseño para la Fabricación y Producción Automatizada, MALTA Consolider Team, Universitat Politècnica de València, 46022 València, Spain
4 Departamento de Física, Instituto de Materiales y Nanotecnología, MALTA Consolider Team, Universidad de La Laguna, 38200 Tenerife, Spain
* Correspondence: estelina.silva@fc.up.pt
† These authors contributed equally to this work.

Abstract: We report an ab initio study of Sb_2S_3, Sb_2Se_3, and Bi_2S_3 sesquichalcogenides at hydrostatic pressures of up to 60 GPa. We explore the possibility that the *C2/m* , *C2/c*, the disordered *Im-3m*, and the *I4/mmm* phases observed in sesquichalcogenides with heavier cations, viz. Bi_2Se_3, Bi_2Te_3, and Sb_2Te_3, could also be formed in Sb_2S_3, Sb_2Se_3, and Bi_2S_3, as suggested from recent experiments. Our calculations show that the *C2/c* phase is not energetically favorable in any of the three compounds, up to 60 GPa. The *C2/m* system is also unfavorable for Sb_2S_3 and Bi_2S_3; however, it is energetically favorable with respect to the *Pnma* phase of Sb_2Se_3 above 10 GPa. Finally, the *I4/mmm* and the disordered body-centered cubic-type *Im-3m* structures are competitive in energy and are energetically more stable than the *C2/m* phase at pressures beyond 30 GPa. The dynamical stabilities of the *Pnma*, *Im-3m*, *C2/m*, and *I4/mmm* structural phases at high pressures are discussed for the three compounds.

Keywords: density functional theory; high-pressure effects; lattice dynamics

Citation: da Silva, E.L.; Santos, M.C.; Rodríguez-Hernández, P.; Muñoz, A; Manjón, F.J. Theoretical Study of Pressure-Induced Phase Transitions in Sb_2S_3, Bi_2S_3, and Sb_2Se_3. *Crystals* **2023**, *13*, 498. https://doi.org/10.3390/cryst13030498

Academic Editors: Andrei Vladimirovich Shevelkov, Daniel Errandonea and Enrico Bandiello

Received: 23 February 2023
Revised: 8 March 2023
Accepted: 12 March 2023
Published: 14 March 2023

1. Introduction

A great deal of attention has been paid to the family of A_2X_3 sesquichalcogenides in the last decade since the identification of the trigonal tetradymite-like *R-3m* phases of the group-15 sesquichalcogenides Sb_2Te_3, Bi_2Se_3, and Bi_2Te_3 as 3D topological insulators [1,2]. Such topological insulators are a state of quantum matter where the bulk is a trivial insulator, whereas the surface states are topologically-protected conducting states due to time-reversal symmetry and strong spin-orbit coupling. Respective properties allow for potential applications in the fields of spintronics as well as for quantum computing [3].

These sesquichalcogenides have also been well studied in relation to their thermoelectric properties and as phase change materials [4,5].

Stibnite (Sb_2S_3), bismuthinite (Bi_2S_3) and antimonselite (Sb_2Se_3) minerals belong to group-15 sesquichalcogenides. Such systems do not crystallize into the tetradymite-type structure at room conditions, but instead into the orthorhombic U_2S_3-type (*Pnma*) structure (Figure 1b). Several technological applications can be considered for such compounds. These include, applications for photovoltaic solar cells, X-ray computed tomography detectors, fuel cells, biomolecules and gas sensors, solid-state batteries, fiber lasers, and photoelectrochemical devices [6–16].

High-pressure (HP) studies of Sb_2Te_3, Bi_2Se_3, and Bi_2Te_3 have shown that they undergo pressure-induced phase transitions (PTs) to monoclinic *C2/m* and *C2/c* structures, to the disordered solid solution *Im-3m* phase, and to the body-centered tetragonal *I4/mmm*

structure [17–26]. These HP studies have shown a plethora of interesting properties, such as enhanced thermoelectric properties [**? ?**] and superconductivity, which could be of topological nature [29–33]. Therefore, there is a fundamental interest in identifying if the above mentioned HP phases can be associated to group-15 sesquichalcogenides with the *Pnma* structure crystallizing at room pressure. Since the *Pnma* structure has also been identified as a possible HP post-perovskite phase of the (Mg,Fe)SiO_3 and $NaFeN_3$ compounds [34,35], the study of Sb_2S_3, Bi_2S_3 and Sb_2Se_3 at HPs could also provide useful information about the structures and stability of ABO_3 orthorhombic minerals at pressure conditions close to those of the Earth's mantle.

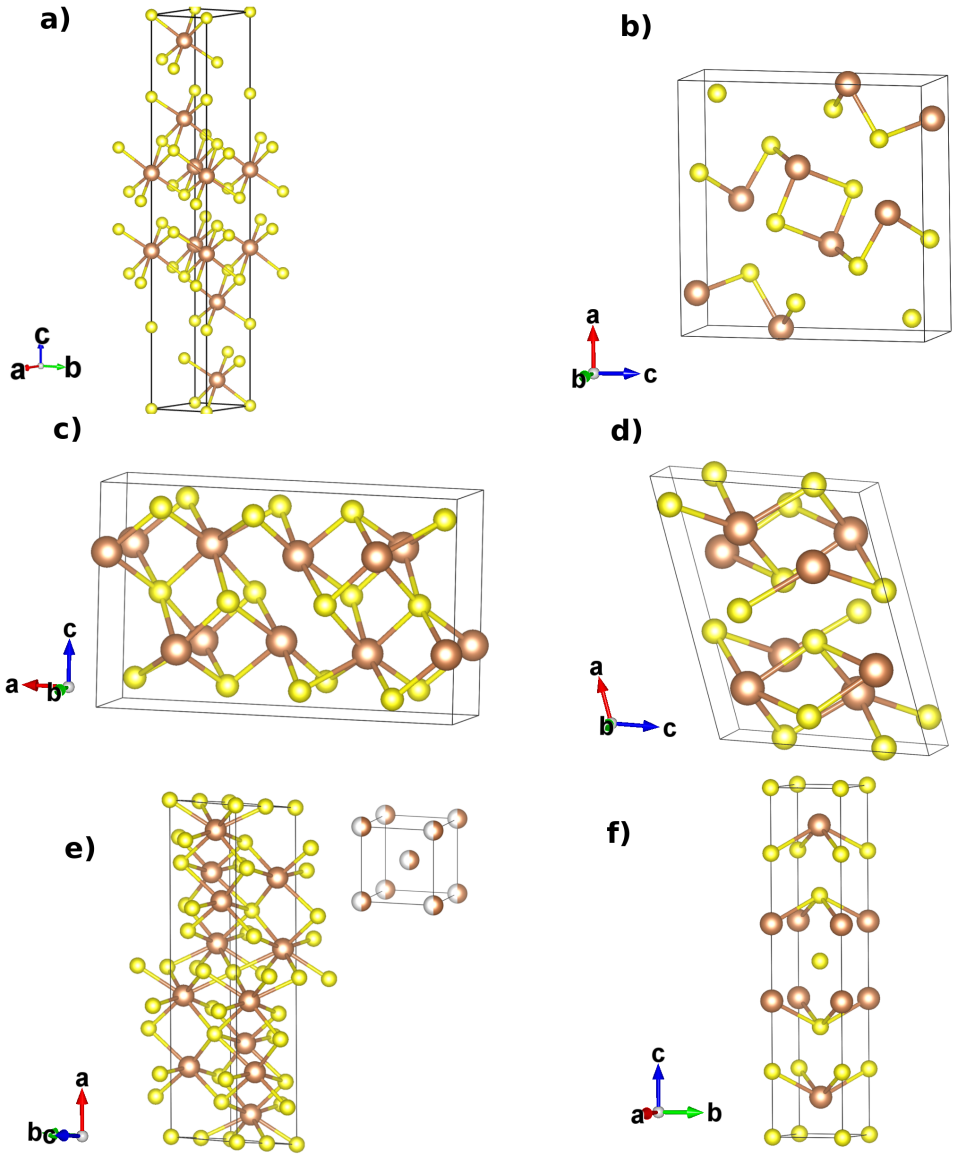

Figure 1. Unit-cell representations of the crystal structures of the *R-3m* (Z = 1) (**a**), *Pnma* (Z = 4) (**b**), *C2/m* (Z = 2) (**c**), *C2/c* (Z = 2) (**d**), the *C2/m* 9-/10-fold structure used to model the disordered bcc-type *Im-3m* phase (Z = 2) (**e**), and the *I4/mmm* (Z = 1) (**f**), and A_2X_3 sesquichalcogenide structures (A = Sb, Bi; X = S, Se). The A cations and X anions are shown as brown and yellow spheres, respectively.

Initial experimental HP studies of Sb_2S_3, Bi_2S_3, and Sb_2Se_3 have shown that the *Pnma* structure is stable under compression, with first-order PTs occurring at around 50 GPa [36–41]. A comparative study between experimental and theoretical analysis suggested that the *Pnma* structure of the three U_2S_3-type sesquichalcogenides should actually

be stable up until 50 GPa [39]. Moreover, another work has reported that the crystalline *Pnma* phase for Sb_2Se_3 is in fact stable even at 70 GPa [**?**]. Curiously enough, HP studies have found that *Pnma*-type Sb_2Se_3 becomes a topological superconductor at around 10 GPa and at a low temperature value of 2.5 K [43], exhibiting highly conducting spin-polarized surface states, and similar to what occurs for Bi_2Se_3 [44]. Moreover, HP superconductivity has been recently found in amorphous Sb_2Se_3 and attributed to the crystallization of the material in a phase with possible "metavalent" bonding as that present in tetradymite-like Sb_2Te_3, Bi_2Se_3, Bi_2Te_3 [45,46].

It must be noted, however, that some experimental HP studies have suggested that several first- and second-order PTs occur for Sb_2S_3 up to 50 GPa [47–49]. Furthermore, it has also been suggested that the HP phases of Sb_2S_3 could be similar to those observed for heavier sesquichalcogenides such as Bi_2Se_3, Bi_2Te_3, and Sb_2Te_3. Moreover, a theoretical study of Bi_2S_3 at HP predicts the system to be unstable under compression, and decomposing into another stoichiometric system [50]. Therefore, there remains the question for whether the different structural phases (*C2/m*, *C2/c*, and disordered *Im-3m* and *I4/mmm*) observed for heavier cation sesquichalcogenides could be observed at HP on the three U_2S_3-type minerals, and at different pressure conditions.

In this work, we report theoretical simulations between 0 GPa and 60 GPa of the *Pnma* and hypothetical *R-3m*, *C2/m*, and *C2/c*; and the disordered *Im-3m* and *I4/mmm* phases for Sb_2S_3, Sb_2Se_3, and Bi_2S_3 (Figure 1), with a view to assessing which, if any, are likely to be observed at HP. This work complements a previous study in which we examined the stability of the tetradymite-like (*R-3m*) phase with respect to the *Pnma* phase, up until 10 GPa, for the three U_2S_3-type minerals [51].

2. Theoretical Methodology

The six studied crystalline phases (*Pnma*, *R-3m*, *C2/c*, *C2/m*, disordered *Im-3m*, and *I4/mmm*) for Sb_2S_3, Bi_2S_3, and Sb_2Se_3 were simulated within the framework of density-functional theory (DFT) [52]. The Vienna Ab initio Simulation Package (VASP) package [53] was used within the projector augmented-wave (PAW) scheme. The datasets included six valence electrons for S[$3s^2 3p^4$] and Se[$4s^2 4p^4$], and 15 valence electrons for Sb[$4d^{10} 5s^2 5p^3$] and Bi[$5d^{10} 6s^2 6p^3$]. Total energy convergence was achieved with a plane-wave kinetic-energy cut-off of 600 eV. The Perdew-Burke-Ernzerhof parameterization revised for solids (PBEsol), of the generalized-gradient approximation (GGA) exchange-correlation (xc) functional [54], was considered for all the calculations.

The sampling of the Brillouin-zone (BZ) was converged with Γ-centered Monkhorst-Pack [55] grids employing adequate meshes for the different structural phases of the three compounds: *Pnma*-6 × 10 × 6, *R-3m*-12 × 12 × 12, *C2/m*-6 × 12 × 6, *C2/c*-10 × 10 × 8, disordered *Im-3m* (using a *C2/m* conventional cell)-6 × 12 × 12, and *I4/mmm*-12 × 12 × 12.

The *Im-3m* phase is a body-centered cubic (bcc) disordered structure, considered as a disordered solid solution, and it has been theoretically predicted and experimentally found for Bi_2Te_3 [17]. For sesquichacogenides with A_2X_3 stoichiometry, the bcc lattice site (2a Wyckoff position) is randomly occupied by 40% of A cations and 60% of X anions. This means that such a structure is a disordered phase with a mixture of cations and anions randomly sharing the same bcc crystallographic position and forming an A-X substitutional alloy [17]. Due to the theoretical difficulty in simulating the disordered *Im-3m* structure, we have used a 9/10-fold *C2/m* structure (the formation of 9/10 chemical A-X bonds), as was previously employed for Bi_2Te_3 [17] and Bi_2Se_3 [22]. Moreover, it has been observed that the 9/10-fold *C2/m* structure presents a bcc-like structural order, in agreement with the observed XRD patterns [17,49], therefore giving support to employ the calculated intermediate bcc-like monoclinic *C2/m* phase to confirm the experimental presence of the disordered *Im-3m* system.

For the structural relaxations, the atomic positions and the unit-cell parameters were allowed to change during the ionic relaxation, for different volume values. From these relaxations, we obtained the respective external pressure for the specific isotropic volume

compression. The pressure-volume (P-V) curves for all the compounds were fitted to a third-order Birch-Murnaghan equation of state [56,57] to obtain the equilibrium volume, bulk modulus, and respective pressure derivative. The enthalpy (H) curves were computed by considering the relation, $H = E + pV$, where E is the total electronic energy of the system, p is pressure, and V is the volume. The analysis and comparison of the H curves for the different polymorphs provides deep insight regarding the thermodynamic stability of each phase for increasing pressure values, up until the studied pressure range (60 GPa).

Lattice dynamics calculations, within the harmonic approximation, were performed at different pressure points, which were found to be energetically favorable. These were considered for the *Pnma*, the disordered *Im-3m*, and the tetragonal phases. We have also calculated the phonon band structure for the *C2/m* system of Sb_2Se_3 to confirm the dynamical stability at the pressure point where the energetic stability is evidenced (20 GPa). The phonon properties were computed by using the supercell finite-displacement method implemented in the Phonopy package [58], with VASP being used as the second-order force calculator. Supercells were expanded up to $2 \times 4 \times 2$ for the *Pnma* systems, and $2 \times 2 \times 2$ for the disordered and tetragonal phases, enabling the exact calculation of frequencies at the zone center (Γ) and inequivalent zone-boundary wavevectors, which were then interpolated to obtain phonon-dispersion curves.

Since our calculations on the *Pnma* phases for the three compounds under study were in good agreement with the overall data found in the literature [51], we have proceeded in carrying out a theoretical study of the hypothetical *R-3m*, *C2/m*, and *C2/c*; and disordered *Im-3m* and *I4/mmm* phases of Sb_2S_3, Bi_2S_3, and Sb_2Se_3, to probe whether such polymorphs could be energetically competitive under hydrostatic pressure.

3. Results and Discussion

3.1. Energetic Stability

Figure 2a–c shows the pressure-dependence of the enthalpy differences relative to the stable phase at ambient pressure between the six above mentioned phases of Sb_2S_3, Bi_2S_3, and Sb_2Se_3, respectively. The values of the predicted transition pressures between the different phases are summarized in Table 1.

Table 1. Theoretical estimation of the pressure-induced phase transitions of *R-3m* → *Pnma*, *Pnma* → disordered *C2/m*, *C2/m* → disordered *Im-3m*, and *Pnma* → disordered *Im-3m* for the Sb_2Se_3, Sb_2S_3, and Bi_2S_3 compounds (presented in units of GPa).

	Sb_2S_3	**Bi_2S_3**	**Sb_2Se_3**
R-3m → *Pnma*	–	–	4.8 *
Pnma → *C2/m*	–	–	9.9
C2/m → *Im-3m*	–	–	22.1
Pnma → *Im-3m*	35.1	30.1	–

* Ref. [51].

From the enthalpy plots (Figure 2), we observe that:

1. At 0 GPa, the orthorhombic *Pnma* structure is energetically stable for Bi_2S_3 and Sb_2S_3; however, for Sb_2Se_3, it is the trigonal *R-3m* phase that is the most energetically favorable phase at 0 GPa [51].
2. The two monoclinic *C2/c* and *C2/m* phases do not become energetically competitive with the ground-state system over the range of pressures examined. However, an exception occurs for the *C2/m* phase of the Sb_2Se_3 structure, which competes energetically with the *Pnma* polymorph at 9.9 GPa.
3. The bcc-like disordered *Im-3m* structure is the most energetically stable phase at pressures above 35.1, 30.1, and 22.1 GPa for Sb_2S_3, Bi_2S_3, and Sb_2Se_3, respectively.
4. The body-centered tetragonal *I4/mmm* phase, although being quite close in energy to the bcc-like *Im-3m* structure (namely, for Bi_2S_3 close to 30 GPa, and for Sb_2Se3 between

30 and 50 GPa), is never energetically favorable within the studied pressure range, for either of the three studied compounds.

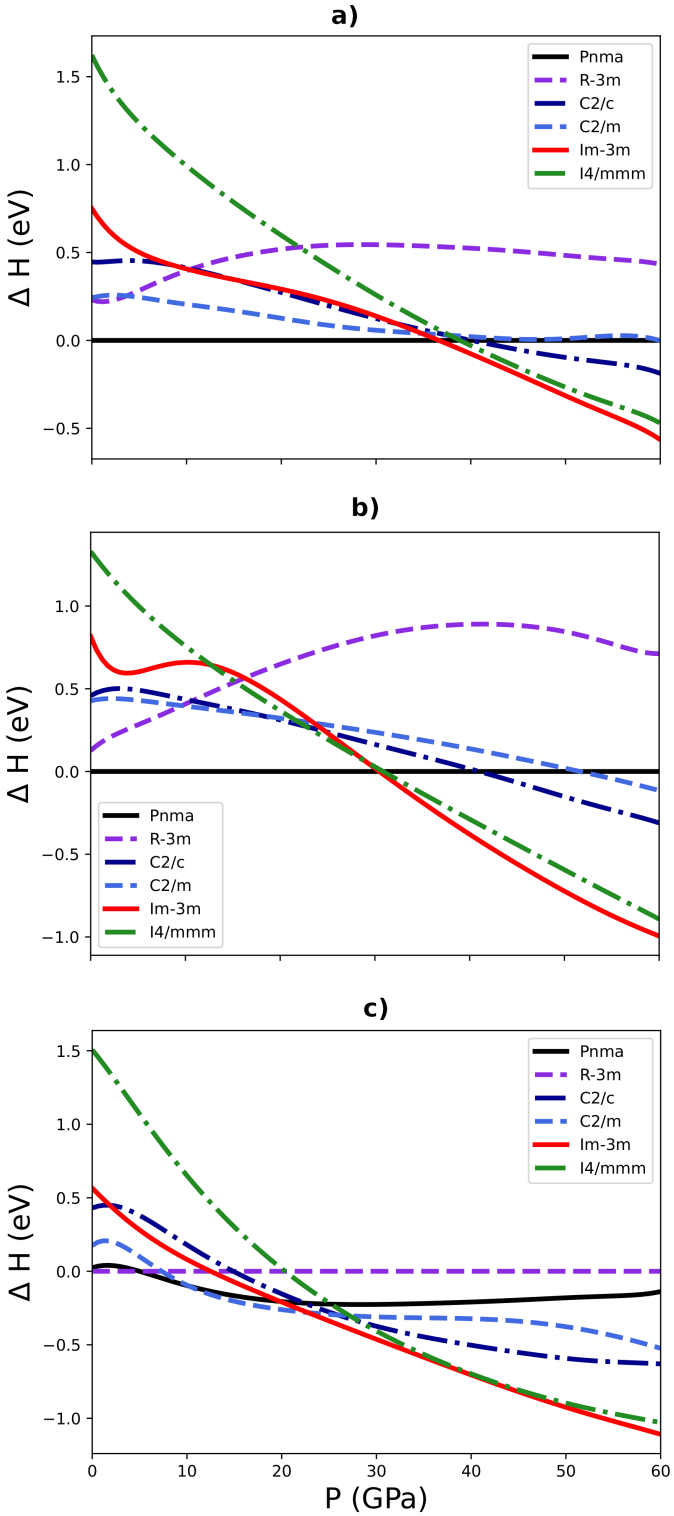

Figure 2. Calculated relative enthalpy vs. pressure curves, for the different possible phases (shown in Figure 1) of Sb_2S_3 (**a**), Bi_2S_3 (**b**), and Sb_2Se_3 (**c**), relative to the lowest-energy phase at ambient pressure: the *Pnma* phase for Sb_2S_3 and Bi_2S_3, and the *R-3m* phase for Sb_2Se_3.

With respect to the first point, referring to Bi_2S_3 and Sb_2S_3, our calculations predict that the *Pnma* structure is energetically the most stable phase, up to 30 GPa, and in good agreement with experimental evidences that show the observation of this phase, both at room and also at HP conditions [30–33,45,46]. Surprisingly, however, our simulations indicate that the Sb_2Se_3 *R-3m* phase is the most stable polymorph at pressures below 4.8 GPa; being both the *Pnma* and *R-3m* phases, energetically competitive between 0 and 4.8 GPa [51].

Regarding the second point, our analysis further shows that the two monoclinic *C2/c* and *C2/m* phases are never energetically competitive in the three compounds throughout the studied pressure range up to 60 GPa; with the exception of the *C2/m* phase of the Sb_2Se_3 close to 10 GPa. These results are consistent with experimental analysis obtained from Refs. [30–33,45,46], in which no PT had been observed for the Sb_2S_3 and Bi_2S_3 systems up until ∼50 GPa. However, the respective results are not consistent with three recent studies reporting evidences of PTs in Sb_2S_3 [47–49]. A PT to an unknown phase was claimed to occur at around 15 GPa [47,48], and several transitions were also reported between 10 and 25 GPa, and tentatively proposed to be the *R-3m*, *C2/c*, and *C2/m* structural phases [49]. In this context, it must be stressed that our calculations are performed for pure hydrostatic conditions; therefore, it is not expected that a complete agreement occurs with experiments if non-hydrostatic conditions are considered for the experiments.

As for the third point, from a thermodynamic point of view, our results indicate that the bcc-like disordered *Im-3m* phase, initially identified for Bi_2Se_3, Bi_2Te_3, and Sb_2Te_3 [17,19,22], seems to be energetically favorable at HP for our three materials of interest. These results are consistent with the observation of such a phase at around 50 GPa for Sb_2Se_3 [36] and above 25 GPa for Sb_2S_3 [47–49]. However, our results do not agree with those found for Bi_2S_3 [37,40], for which a disorder, attributed mostly to a pressure-induced amorphization (PIA), has been observed above 50 GPa. Notably, PIA in Bi_2S_3 is consistent with a recent theoretical work that claims that a respective system is unstable above 31.5 GPa, decomposing into a mixture of BiS_2 and BiS compounds [50]. In this context, it must be stressed that the existence of a bcc-like structure at HP is not only expected for A_2X_3 sesquichalcogenides, but also for AX (A=Ge,Sn,Pb) chalcogenides [**?** **?**]. All these compounds have in common the property of being cataloged as evidencing metavalent bonding at room pressure, such as SnTe, PbS, PbSe, PbTe, Sb_2Te_3, Bi_2Se_3, or Bi_2Te_3 [46]; or as being compounds with p-type covalent bonds that develop metavalent bonding at HP when approaching a six-fold coordination, such as GeSe, SnSe, As_2S_3, and also U_2S_3-type sesquichalcogenides [61,62], and ultimately, they will reach eight-fold coordination typical of bcc-like metals at very HP.

With respect to the fourth point, the *I4/mmm* structure was firstly proposed for Bi_2Se_3 by combining experimental and theoretical data [25]. It was found that the structural phase transition pathway for Bi_2Se_3 followed the sequence: *R-3m* → *C2/m* → *C2/c* → *I4/mmm*, when the quasi-hydrostatic pressure was considered. The *C2/c* phase would, however, be suppressed when nonhydrostatic pressure conditions are taken into account [25]. These results are also compatible with Raman analysis and XRD data performed on Bi_2Se_3, where it was evidenced that the stability of the *I4/mmm* phase was up to 81.2 GPa [24]. Moreover, it has also been claimed [26], that the alloying of Bi_2Se_3 with Bi_2Te_3 enables transitions to occur from the monoclinic phases, up to the disordered *Im-3m* at ∼19 GPa, which then would be surpassed energetically by the tetragonal *I4/mmm* polymorph at ∼23 GPa. Curiously enough, the energetic competition between the *C2/m*, *C2/c*, and *I4/mmm* phases is observed at HP for all three U_2S_3-type sesquichalcogenides (if we discard the disordered *Im-3m* phase), and the *I4/mmm* structure would indeed be energetically the most favorable polymorph at very HP. However, the disordered *Im-3m* phase is always energetically more competitive than *I4/mmm* for the U_2S_3-type sesquichalcogenides, and so this latter phase is, *a priori*, not expected to be observed at HP.

Finally, we have to mention that we have also performed the enthalpy calculations by employing two further xc functionals, in order to confirm the present theoretical data (see Appendix A). The employed functionals were the PBE-D2 method of Grimme (which takes

into account the dispersion correction term) [63], and LDA [64]. From the analysis of the plots (Figures A1 and A2) we can infer similar energetic trends of the six polymorphs; however, mild differences are observed between the two competing phases of the disordered *Im-3m* and *I4/mmm*—detailed discussion is found in Appendix A.

In summary, the agreement of our results regarding the observation of the disordered *Im-3m* phase for Sb_2Se_3 and Sb_2S_3, but not for Bi_2S_3, suggests that thermodynamic stability is not sufficient to explain the lack of the HP disordered phase for the latter compound. In the following section, we discuss the dynamical stability of the *Pnma*, *C2/m*, *Im-3m*, and *I4/mmm* phases as a function of pressure, in order to provide a deeper understanding regarding this question.

3.2. Dynamical Stability

Energetic stability is a necessary, but it is not a sufficient condition for a structural phase to be synthetically accessible. One should also probe the dynamical stability of the system, which requires the study of the phonon frequencies. If imaginary frequencies emerge (as represented by negative frequencies in the phonon dispersion curves), we can analyze the results by considering that the system is at a potential-energy maximum (transient state), undergoing a phase transition, and therefore cannot be kinetically stable at the given temperature and/or pressure conditions [65–70].

In this section, we consider the phonon properties of different phases for the three compounds, which were observed to be energetically the most favorable (Figure 2) at different pressure values, namely:

1. The *C2/m* phase of Sb_2Se_3 at 20 GPa.
2. The disordered bcc-type *Im-3m* phase of the three compounds above 30 GPa.
3. The *Pnma* phase of the three compounds at 50 GPa.
4. The *I4/mmm* phase of the three compounds at HP.

3.2.1. The *C2/m* Phase of Sb_2Se_3 at 20 GPa

By analyzing the enthalpies as a function of pressure (Figure 2), we observe that the *C2/m* phase in Sb_2Se_3 is thermodynamically the most stable phase between 10 and 20 GPa. In order to confirm the dynamical stability, we have performed the phonon dispersion curves of respective system at 20 GPa (Figure 3). The dispersion curves do not evidence any imaginary modes; therefore, we may conclude that the *C2/m* phase in Sb_2Se_3 is dynamically stable in this pressure range and could potentially be observed after the *Pnma* phase, although it has not yet been experimentally observed [36].

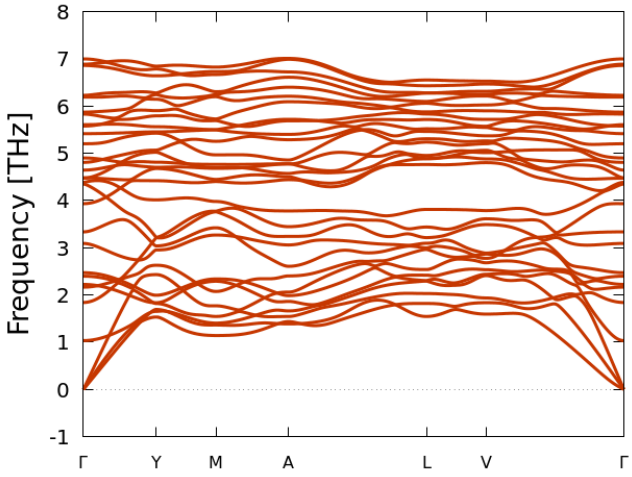

Figure 3. Harmonic phonon dispersion curves of the *C2/m* phase of the Sb_2Se_3 compound at 20 GPa.

3.2.2. The Disordered bcc-Type *Im-3m* Phase of the Three Compounds above 30 GPa

To assess the possibility of dynamical stability for the disordered *Im-3m* phases of the three compounds at HP, we have evaluated the phonon dispersion curves at pressure values of 30 GPa, which is close to the transition pressures observed in Figure 2; and at higher pressures of 50 (Sb_2Se_3) and 60 GPa (Sb_2S_3, Bi_2S_3).

As illustrated in Figure 4, all three disordered structures at 30 GPa show imaginary modes along the dispersion curves, thus indicating that these structures are dynamically unstable at this pressure range.

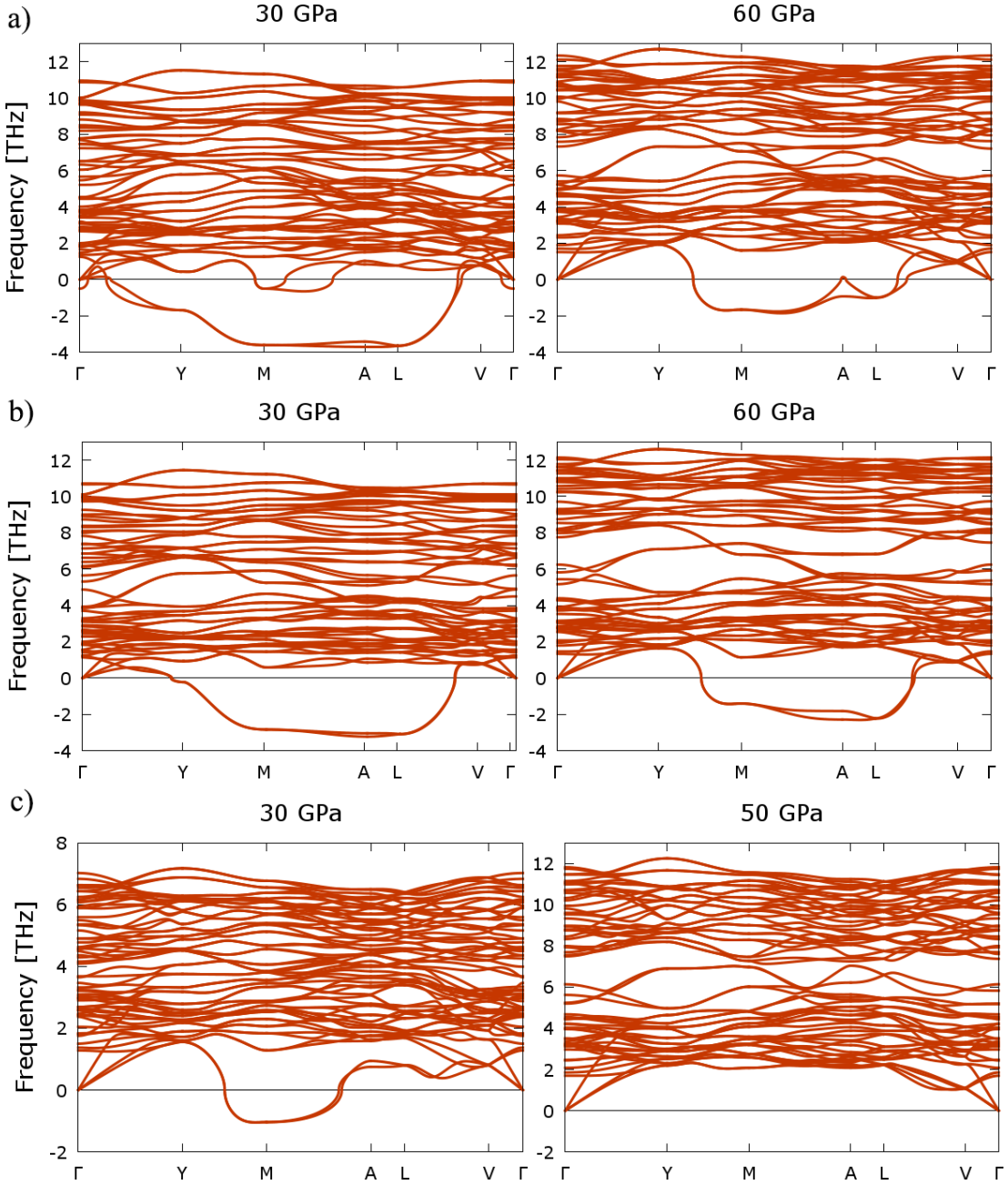

Figure 4. Harmonic phonon dispersion curves of the disordered bcc-like *Im-3m* phases of Sb_2S_3 (**a**), Bi_2S_3 (**b**), and Sb_2Se_3 (**c**); and calculated at 30 GPa (**left**), and 50 (Sb_2Se_3) or 60 GPa (Sb_2S_3 and Bi_2S_3; **right**). The BZ **q**−vector description represents the *C2/m* space−group, according to the symmetry of the employed cell.

The phonon dispersion curves of Sb_2S_3 and Bi_2S_3 still present imaginary modes at 60 GPa (Figure 4), thus indicating that neither compound is likely to adopt this phase up to this pressure range. We note, however, that the dynamical instabilities found for Sb_2S_3 and Bi_2S_3 both decrease (the imaginary, soft modes shift to higher frequency values, towards positive values) with increasing pressure, suggesting that this phase could in principle become stable at pressures above 60 GPa. In this context, we must note that Efthimiopoulos et al. [37] had observed a pressure-induced amorphization above 50 GPa for Bi_2S_3; however, the authors were not able to identify the phase to be the disordered *Im-3m* structure, even at 65 GPa. On the other hand, the experimental data for Sb_2S_3, suggests that the disordered bcc-like phase exists between 28.2 and 50.2 GPa [49]. However, it must be noted that experimental measurements detailed in Ref. [49] were carried out under non-hydrostatic behavior due to the employed pressure-transmitting medium.

Finally, our calculations suggest that the *Im-3m* phase becomes dynamically stable in Sb_2Se_3 already at 50 GPa; a result that is in agreement with the experimental observation of this phase at around 50 GPa [36].

In the light of the above results regarding the disordered *Im-3m* phase of Sb_2S_3, Bi_2S_3, and Sb_2Se_3, we can speculate that the stability of the disordered solid solution in group-15 sesquichalcogenides seems to be related to the sizes of cations and anions. Since the *Im-3m* phase is consistently being evidenced at HP for sesquichalcogenides with heavier cations and anions (Sb_2Se_3, Sb_2Te_3, Bi_2Se_3, and Bi_2Te_3), the observation of such a HP phase could be related to the radius sizes [71] of Se, Te, Sb, and Bi (atomic radii: $r_{Se} = 117$, $r_{Te} = 137$, $r_{Sb} = 141$, and $r_{Bi} = 182$ pm, respectively). Stemming on these values, we can infer that the disordered solid solutions are energetically favorable in sesquichalcogenides if the atomic radii of the cation and anion differ by less than $\sim$ 65 pm, or if the size ratio between them is smaller than $\sim$1.55 (case of Bi_2Se_3). In this context, Sb_2S_3, which shows a radius difference of between r_{Sb} and r_S of 37 pm (141 − 104 = 37 pm) and a size ratio of 1.35, meets the criteria for the observation of the disordered *Im-3m* phase at HP. However, Bi_2S_3, which evidences a larger radius difference (78 pm) and ratio (1.75) between B and S, does not satisfy the above criteria. Such results would therefore be consistent with the amorphous phase observed for Bi_2S_3 at HP [37,40].

Finally, it must be considered, and as suggested in Ref. [17], that the atomic radii between the anion and cation tend to become approximately equal at HP due to a higher probability of charge transfer from cation to anion. Therefore, HP inherently creates a favorable environment for the disordered solid solutions due to the decrease in the difference between the cation and anion atomic radii. This means that we cannot discard that the disordered solid solution in Bi_2S_3 could occur at very HP values, namely, when the difference between the two radii decreases below 65 pm and when the ratio decreases below 1.55.

3.2.3. The *Pnma* Phase of the Three Compounds at 50 GPa

In order to study the dynamical stability of the well known low-pressure *Pnma* phase at HP, we present in Figure 5 the phonon dispersion curves of the respective phase for Sb_2S_3, Bi_2S_3, and Sb_2Se_3 at 50 GPa.

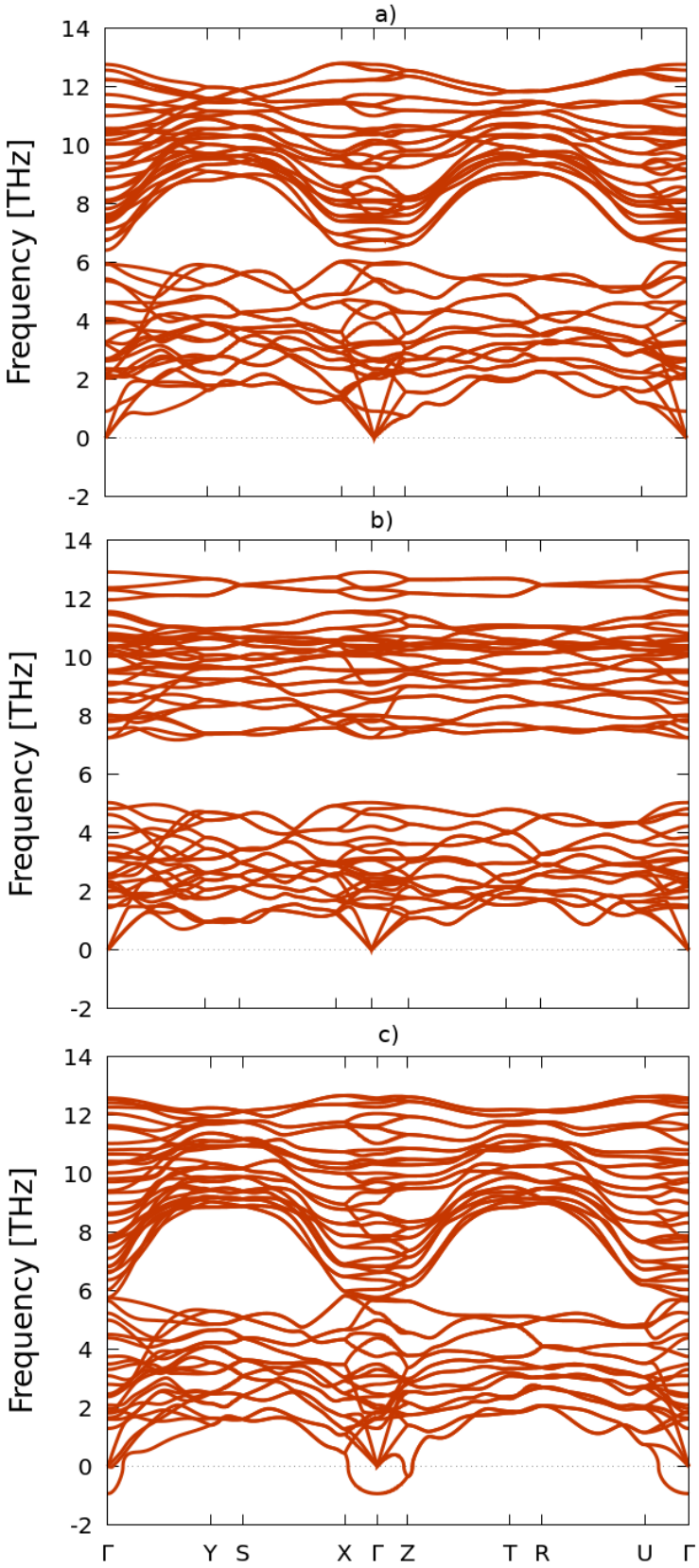

Figure 5. Harmonic phonon dispersion curves of the *Pnma* phase of Sb_2S_3 (**a**), Bi_2S_3 (**b**), and Sb_2Se_3 (**c**), calculated at 50 GPa.

Curiously enough, we find that the *Pnma* phase for Sb_2Se_3 is already unstable at 50 GPa; therefore, a PT should occur at smaller pressures to the *C2/m* phase, and ultimately, to the disordered *Im-3m* phase, as previously commented. On the other hand, the *Pnma* phase for Sb_2S_3 and Bi_2S_3 is still dynamically stable at 50 GPa, although thermodynamically, it is not the most stable phase (Figure 2). These results, together with the dynamical instability observed for the disordered phase of Sb_2S_3 and Bi_2S_3 at 50 GPa (Figure 4) and the thermodynamic instability of the *C2/m* and *C2/c* phases, suggest that only the *Pnma* structure should be observed up to 50 GPa for both compounds, unless there is a decomposition, as theoretically predicted for Bi_2S_3 [50].

3.2.4. The *I4/mmm* Phase of the Three Compounds at HP

By considering the enthalpy curves of the three compounds (Figure 2), we can infer that the *I4/mmm* phase is very close in energy with the disordered *Im-3m* system at pressures above 30 GPa. We therefore have carried out phonon calculations to probe the dynamical stability of this phase, and for all three compounds.

With regard to the Sb_2S_3 system, we observe that only at 60 GPa is the *I4/mmm* structural phase dynamically stable (Figure 6). Below this pressure value, imaginary modes are observed in the vicinity of the Γ-point, which harden for increasing pressure points. This result, together with the dynamic instability of the disordered *Im-3m* phase still at 60 GPa, suggests that both the *I4/mmm* and *Im-3m* structures are not expected to be observed at pressures below 60 GPa; however, any of these systems could potentially be observed above this pressure range.

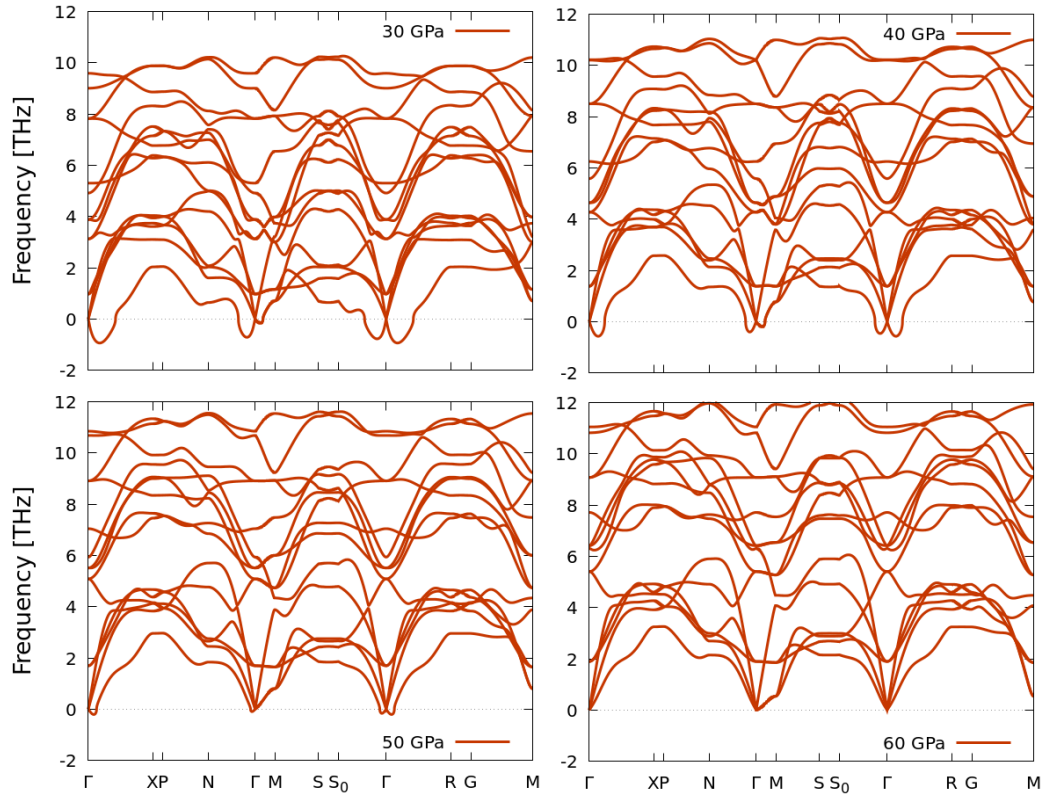

Figure 6. Harmonic phonon dispersion curves of the *I4/mmm* phase of the Sb_2S_3 compound between 30 and 60 GPa.

With respect to the Bi_2S_3 compound (Figure 7), we observe that the *I4/mmm* phase is already dynamically stable at 50 GPa, maintaining the stability at 60 GPa. Therefore, the *I4/mmm* phase could in fact be observed at above 40 GPa, if there was no sample decomposition, as theoretically predicted [50].

Finally, we observed that the the tetragonal *I4/mmm* phase for Sb_2Se_3 is only dynamically stable at 40 GPa (Figure 8), since there is a localized imaginary mode at the high-symmetry *M*-point, at any other pressure value. These results differ from the remaining two S-based compounds, and evidence that the disordered *Im-3m* phase will be the only (thermodynamically and dynamically) stable phase for the Sb_2Se_3 compound at very HP (since the *Pnma* is also unstable at 50 GPa, Figure 5c), and as discussed in the previous subsection.

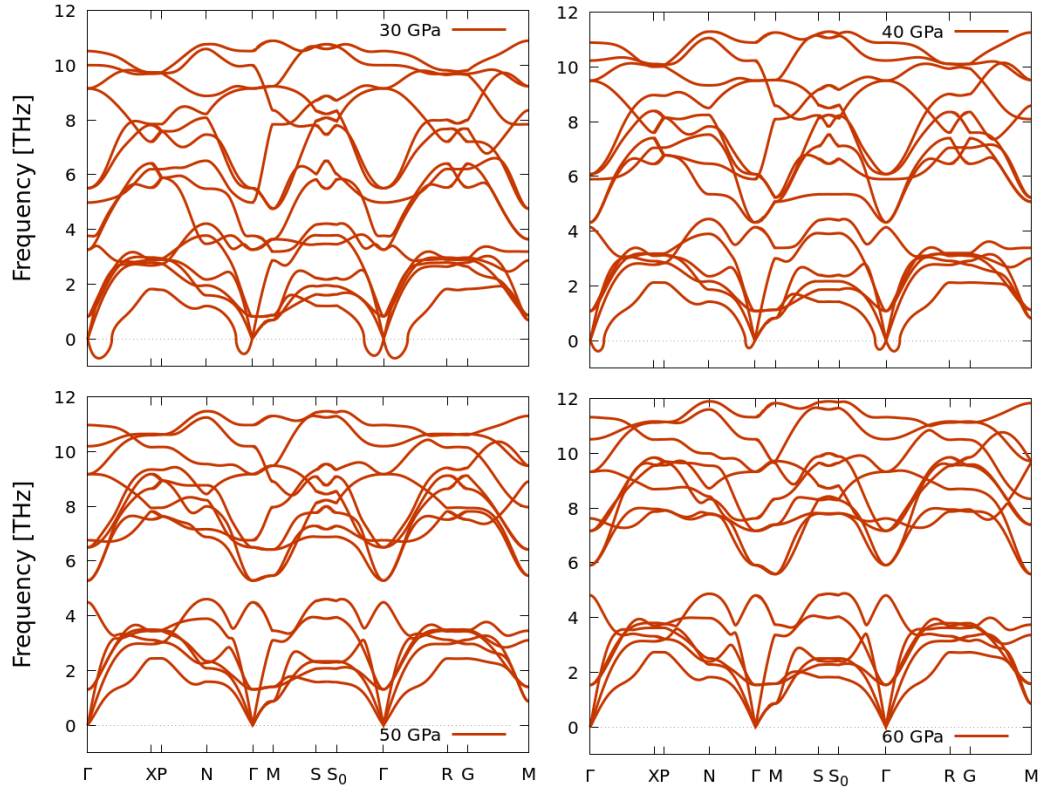

Figure 7. Harmonic phonon dispersion curves of the *I4/mmm* phase of the Bi_2S_3 compound between 30 and 60 GPa.

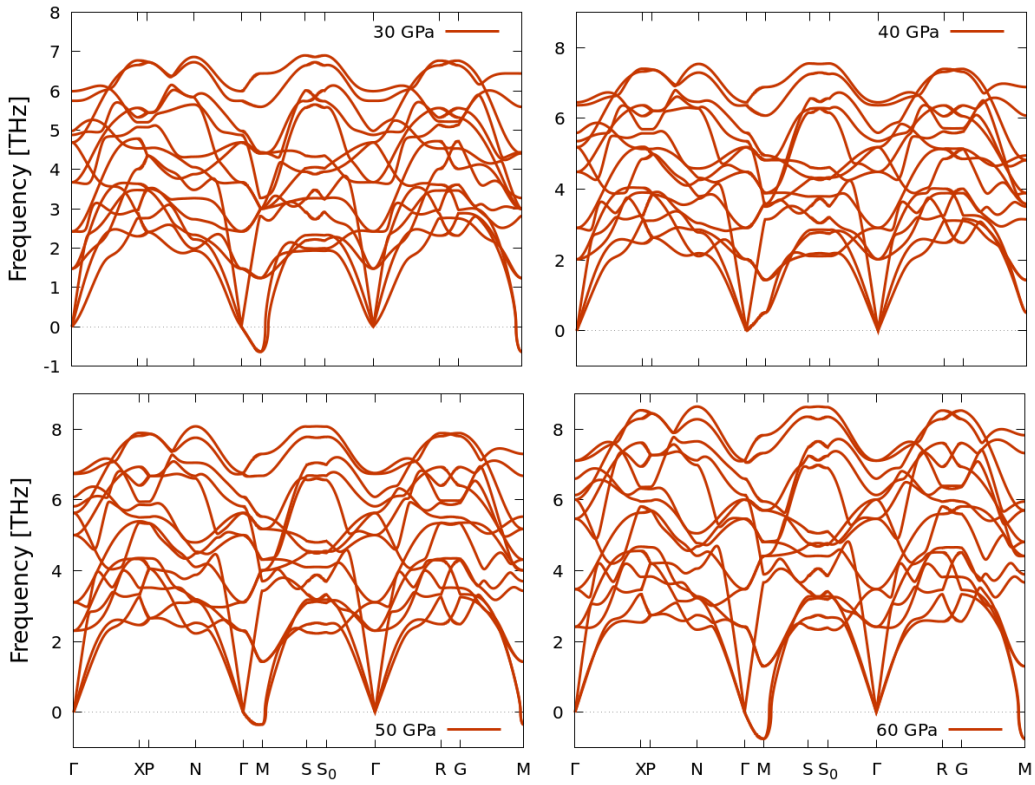

Figure 8. Harmonic phonon dispersion curves of the *I4/mmm* phase of the Sb_2Se_3 compound between 30 and 60 GPa.

4. Conclusions

We have carried out a comprehensive set of total energy and lattice dynamics calculations in order to investigate the stabilities of six possible structural phases, viz. *Pnma*, *R-3m*, *C2/m*, and *C2/c*; and disordered *Im-3m* and *I4/mmm* for the Sb_2S_3, Bi_2S_3, and Sb_2Se_3 sesquichalcogenides under hydrostatic pressures up to 60 GPa. Our theoretical results have been commented in the light of the available experimental data.

We find that the *Pnma* phase is energetically more stable at room pressure for the Sb_2S_3 and Bi_2S_3 compounds. Curiously, the trigonal *R-3m* phase is the most energetically favorable phase for Sb_2Se_3 at 0 GPa, although from an experimental perspective, this compound is synthesized in the *Pnma* phase. In fact, we find that the *Pnma* phase is dynamically stable for Sb_2S_3 and Bi_2S_3 up to 50 GPa, but not for Sb_2Se_3 at this pressure value.

From our calculations, we observe that the monoclinic *C2/m* and *C2/c* systems for the three compounds are energetically less favorable throughout the studied pressure range, and they are not expected to be observed at HP under hydrostatic conditions, except for Sb_2Se_3 between 10 and 20 GPa. Moreover, the *C2/m* phase of Sb_2Se_3 is dynamically stable at 20 GPa, so a pressure-induced phase transition from the *Pnma* to the *C2/m* system could be observed between 10 and 20 GPa under hydrostatic conditions.

The disordered bcc-like *Im-3m* phase is predicted to be the most energetically stable phase above 35, 30, and 22 GPa for Sb_2S_3, Bi_2S_3, and Sb_2Se_3, respectively; however, this structure is dynamically unstable for Sb_2S_3 and Bi_2S_3 up to 60 GPa, and for Sb_2Se_3 up to 50 GPa. Therefore, this HP phase is expected to occur for Sb_2Se_3 above 50 GPa, in good agreement with experiments, and perhaps above 60 GPa for the other two compounds.

With respect to the *I4/mmm* phase, we have learned that the structure is not energetically competitive with the *Im-3m* phase, throughout the studied pressure range, and for the three compounds; however, this phase is close in energy to the *Im-3m* phase for Bi_2S_3 at 30 GPa, and for Sb_2Se_3, close to 38 GPa. On the other hand, the *I4/mmm* system is dynamically stable for Bi_2S_3 above 50 GPa, and for Sb_2Se_3, quite close to 40 GPa. Therefore,

this phase could potentially be observed for the former compound at HP; however, not for Sb_2Se_3.

Curiously enough, we must mention that through symmetry analysis, the *I4/mmm* → *Fmmm* → *C2/m* structural transition pathway may occur as a second-order phase transition. We have, however, not considered the intermediate *Fmmm* system, since, and to the best of our knowledge, such a phase has not yet been experimentally observed for sesquichalcogenides at HP, and therefore, respective analysis would be out the scope of the present work.

We hope that this work will stimulate further investigation of the sesquichalcogenides at HP in order to clarify which pressure-induced phase transitions are observed under hydrostatic and non-hydrostatic conditions.

Author Contributions: E.L.d.S., M.C.S., P.R.-H., and A.M. performed the ab initio calculations. F.J.M. supervised the work and comparison with experimental data. E.L.d.S. and F.J.M. wrote the manuscript. All authors have read and agreed to the published version of the manuscript.

Funding: This publication is part of the Project MALTA Consolider Team network (RED2018-102612-T), financed by MINECO/AEI/10.13039/501100003329; by I+D+i project PID2019-106383GB-42/43, financed by MCIN/AEI/10.13039/501100011033; by projects PROMETEO CIPROM/2021/075 (GREENMAT) and MFA/2022/025 (ARCANGEL), financed by Generalitat Valenciana; and by the European Union Horizon 2020 research and innovation programme under the Marie Sklodowska-Curie grant, agreement No. 785789-COMEX.

Data Availability Statement: The data that support the work presented within this paper are available from the corresponding author upon reasonable request.

Acknowledgments: E.L.d.S acknowledges the High Performance Computing Chair—an R&D infrastructure (based at the University of Évora; PI: M. Avillez), endorsed by Hewlett Packard Enterprise, and involving a consortium of higher education institutions, research centers, enterprises, and public/private organizations; and the Portuguese Foundation of Science and Technology with the CEEC individual fellowship, 5th edition, with Reference 2022.00082.CEECIND.

Conflicts of Interest: The authors declare no conflict of interest.

Appendix A. Comparison of Enthalpy vs. Pressure Behavior for Different Exchange-Correlation Functionals

In order to confirm the enthalpy variation as the pressure increases for the six studied phases presented in Figure 2, and obtained by employing the PBEsol functional, we observe that the energetic trends are functional-independent. In Figures A1 and A2, we present enthalpy results carried out by considering the PBE-D2 and the LDA functional, respectively. For PBE-D2 (Figure A1), the transition pressures are very close to those obtained with PBEsol. Moreover, for the Sb_2Se_3 system, the energetic trends are also comparable to those of PBEsol, namely, that the *R-3m* phase is energetically the most stable at room pressure, and that the *C2/m* phase shows a small interval range of stability before the disordered *Im-3m* phase takes over the energetic configurational space. The *I4/mmm* system is energetically competitive, with the disordered phase at a slightly lower pressure range when compared to the results obtained with PBEsol. For Sb_2S_3 and Bi_2S_3, the tetragonal *I4/mmm* phase becomes energetically the most stable at pressures close to 60 GPa. The results obtained with the LDA functional (Figure A2) also show similar trends; however, the transition pressures are slightly higher than for PBEsol. Moreover, a competition between the two monoclinic phases and *I4/mmm* seems to occur in Sb_2Se_3 slightly, before the latter phase becomes the most stable phase. At around 60 GPa, the disordered phase stabilizes, becoming the most stable structure for Sb_2Se_3. In addition, for the Bi_2S_3 compound, we observe a pressure range, at which the *I4/mmm* becomes energetically the most stable (∼30–45 GPa), which then is energetically taken over by the disordered *Im-3m* phase at above 45 GPa.

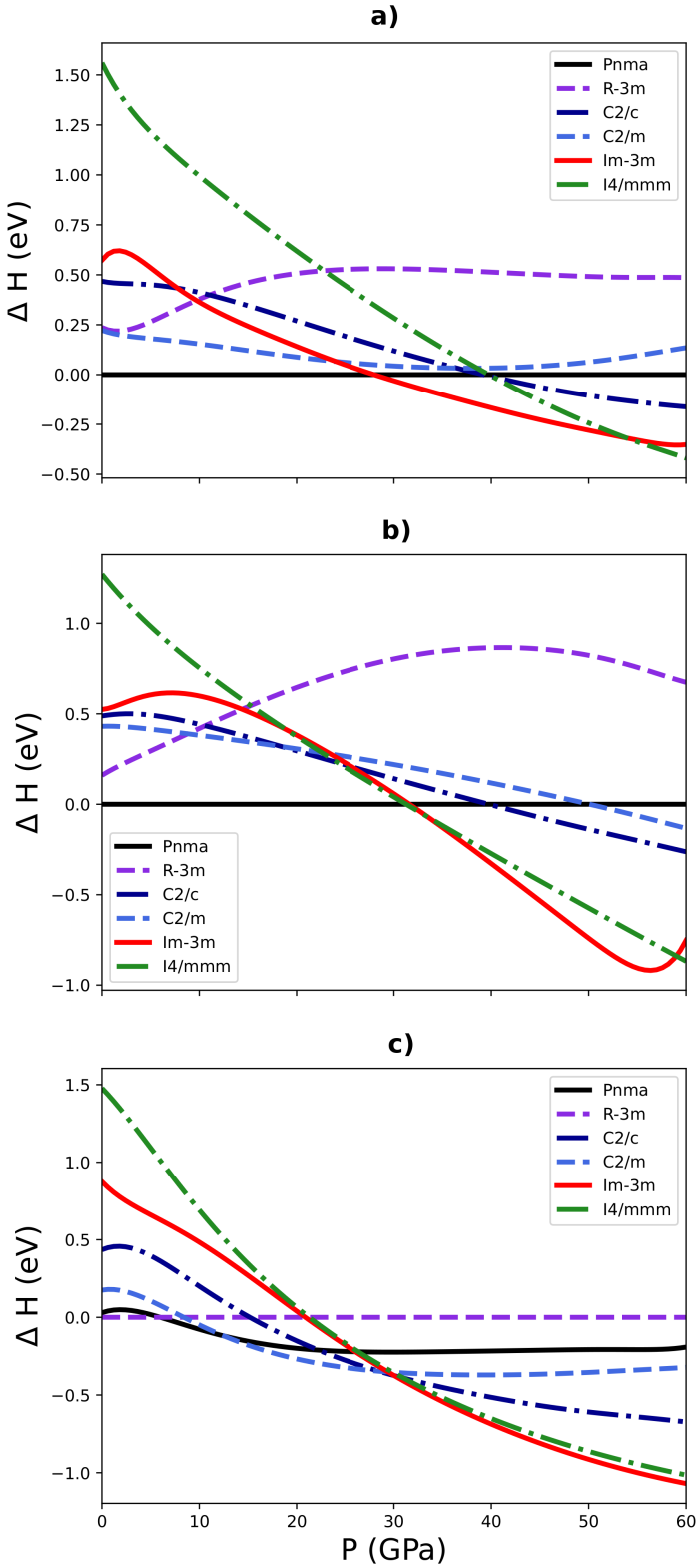

Figure A1. PBE+vdW enthalpy vs. pressure curves, for the different possible phases (shown in Figure 1) of Sb_2S_3 (**a**), Bi_2S_3(**b**), and Sb_2Se_3 (**c**), relative to the lowest-energy phase at ambient pressure: the *Pnma* phase for Sb_2S_3 and Bi_2S_3, and the *R-3m* phase for Sb_2Se_3.

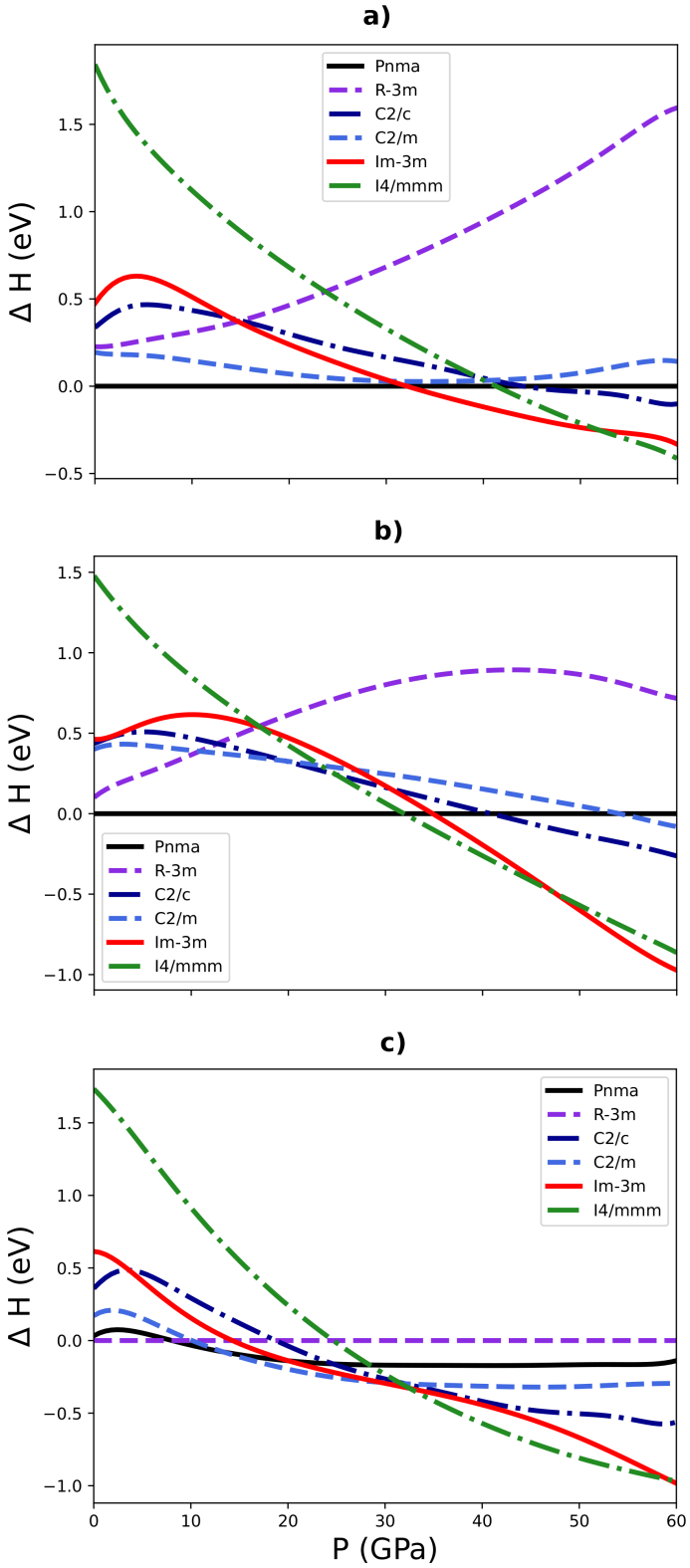

Figure A2. LDA enthalpy vs. pressure curves, for the different possible phases (shown in Figure 1) of Sb_2S_3 (**a**), Bi_2S_3 (**b**), and Sb_2Se_3 (**c**), relative to the lowest-energy phase at ambient pressure: the *Pnma* phase for Sb_2S_3 and Bi_2S_3, and the *R-3m* phase for Sb_2Se_3.

Appendix B. Evolution of the Lattice Parameters of Sb_2S_3, Bi_2S_3, and Sb_2Se_3 as a Function of Pressure

In Tables A1–A3, we present the lattice parameters of the different studied compounds at pressure values where stability (thermodynamic and dynamical) is evidenced. Since the *C2/c* structure is never stable throughout the studied pressure range, we do not present the respective theoretical values for any of the compounds. As for Sb_2S_3 and Bi_2S_3, we only present the lattice parameters related to the *Pnma* phase, at 0 and 30 GPa, since this is the pressure range for which the structure is energetically more favorable; and where none of the remaining phases satisfy both of the stability conditions that we mentioned previously.

Table A1. Theoretical estimation (PBEsol) of the lattice parameters of the Sb_2S_3 compound, for the *Pnma* structural phase, for different pressure values, at which the system is both energetically and dynamically stable (presented in units of Å).

Sb_2S_3	0 GPa	10 GPa	20 GPa	30 GPa
a_0	11.24	10.30	10.02	9.82
b_0	3.83	3.72	3.63	3.58
c_0	10.91	10.24	9.83	9.53

Table A2. Theoretical estimation (PBEsol) of the lattice parameters of the Bi_2S_3 compound, for the *Pnma* structural phase, for different pressure values, at which the system is both energetically and dynamically stable (presented in units of Å).

Bi_2S_3	0 GPa	10 GPa	20 GPa	30 GPa
a_0	11.19	10.59	10.38	10.22
b_0	3.96	3.82	3.74	3.67
c_0	10.94	10.32	9.94	9.64

Table A3. Theoretical estimation (PBEsol) of the lattice parameters of the Sb_2Se_3 compound, for the different structural phases that are both energetically and dynamically stable within the range of studied pressures (presented in units of Å).

Sb_2Se_3		
Pnma	10 GPa 15 GPa 20 GPa	a_0 = 10.77, b_0 = 3.83, c_0 = 10.69 a_0 = 10.63, b_0 = 3.77, c_0 = 10.48 a_0 = 10.50, b_0 = 3.72, c_0 = 10.35
R-3m	0 GPa	a_0 = 4.01, c_0 = 28.16
C/2m	20 GPa	a_0 = 13.15, b_0 = 3.55, c_0 = 8.06
disordered *Im-3m*	50 GPa	a_0 = 13.55, b_0 = 4.49, c_0 = 5.50
I4/mmm	40 GPa	a_0 = 3.26, c_0 = 15.84

Appendix C. Mode Mapping of the Disordered *Im-3m* Phase of Sb_2Se_3 at 30 GPa

By observing the phonon dispersion curves of the disordered *Im-3m* phase in Sb_2Se_3 at 30 GPa (Figure 4c), we may notice that the instability mode is localized at a high-symmetry point, the *M*-point, which is defined as being a zone-boundary instability (or anti-ferroelectric instability, resulting in an anti-phase periodic distortion). Since the negative mode is localized, it is therefore possible to map out the anharmonic potential energy surfaces by following the eigenvectors associated with this instability/displacement, and thus, to be able to obtain a lower energy structure corresponding to the minima of the potential energy surface. For these calculations, we use the open-source MODEMAP package [72,73]. A sequence of displaced structures in a commensurate supercell ($1 \times 2 \times 2$) expansion is generated by displacing along the phonon eigenvectors over a range of amplitudes of the normal-mode coordinate Q. The total energies of the "frozen phonon"

structures are evaluated from single-point DFT calculations. The E(Q) curves are then fitted to a polynomial function, with the number of terms depending on the form of the potential well.

The displacements associated with the disordered bcc high-pressure structure result from the condensation of these soft M-modes, leading to a lower energy system and an enlarged primitive unit-cell. The displacement involves two Se atoms at the center of the cell, namely at (0.50000, 0.75000, 0.50000) and (0.50000, 0.25000, 0.50000). Both atoms evidence mild distortions along the x- and z-directions, minimizing the energy to 3.63 meV when compared to the original disordered *Im-3m* phase at $Q = 0$ (Figure A3).

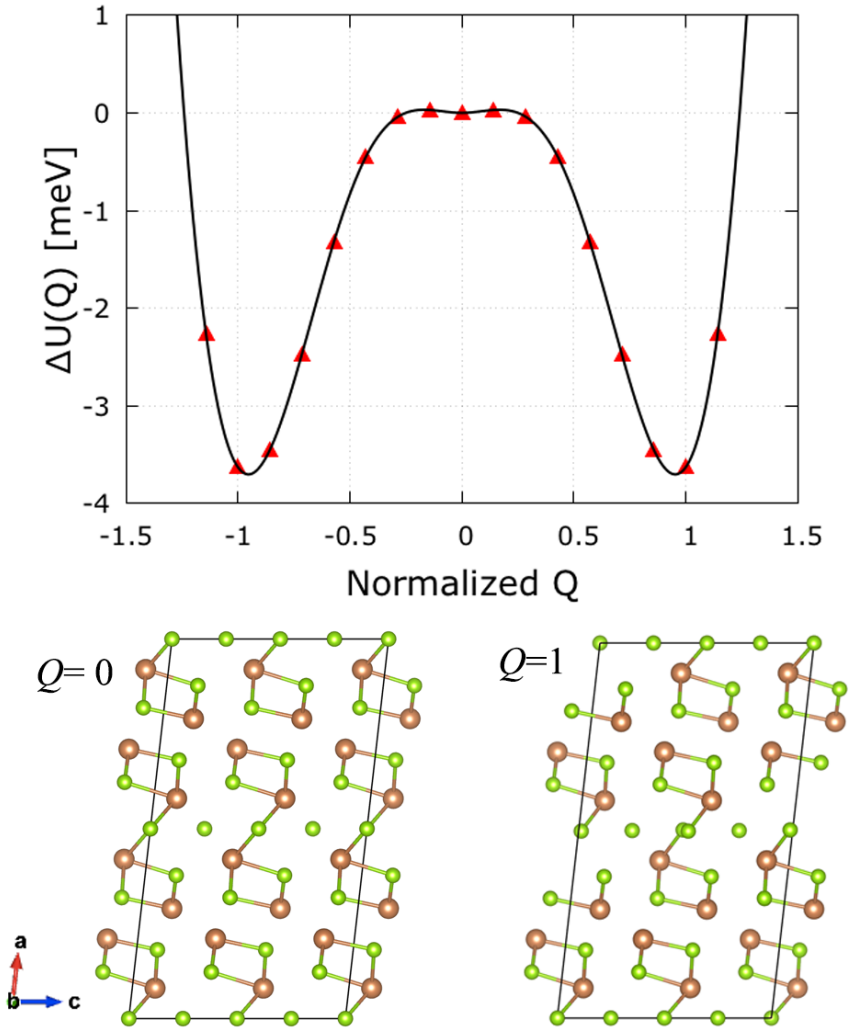

Figure A3. Double −well potential−energy surfaces for the phonon instabilities associated with the high-symmetry M −point negative modes (Figure 4). The normal-mode coordinates Q have been normalized so that the minima are located at $Q = \pm 1$, and the energy differences are those calculated in a $1 \times 2 \times 2$ supercell. The bottom figures represent the structure at Q = 0 (**left**) and at Q = 1 (**right**).

References

1. Chen, Y.L.; Analytis, J.G.; Chu, J.H.; Liu, Z.K.; Mo, S.K.; Qi, X.L.; Zhang, H.J.; Lu, D.H.; Dai, X.; Fang, Z.; et al. Experimental Realization of a Three-Dimensional Topological Insulator, Bi_2Te_3. *Science* **2009**, *325*, 178. [CrossRef]
2. Zhang, H.; Liu, C.X.; Qi, X.L.; Dai, X.; Fang, Z.; Zhang, S.C. Topological insulators in Bi_2Se_3, Bi_2Te_3 and Sb_2Te_3 with a single Dirac cone on the surface. *Nat. Phys.* **2009**, *5*, 438. [CrossRef]
3. Hasan, M.Z.; Kane, C.L. Colloquium: Topological insulators. *Rev. Mod. Phys.* **2010**, *82*, 3045. [CrossRef]
4. Venkatasubramanian, R.; Siivola, E.; Colpitts, T.; O'Quinn, B. Thin-film thermoelectric devices with high room-temperature figures of merit. *Nature* **2001**, *413*, 597. [CrossRef] [PubMed]

5. Martinez, J.C.; Lu, L.; Ning, J.; Dong, W.; Cao, T.; Simpson, R.E. The Origin of Optical Contrast in Sb_2Te_3-Based Phase-Change Materials. *Phys. Status Solidi B* **2020**, *257*, 1900289. [CrossRef]
6. Sa Moon, S.J.; Itzhaik, Y.; Yum, J.H.; Zakeeruddin, S.M.; Hodes, G.; Gräzel, M. Sb_2S_3-Based Mesoscopic Solar Cell using an Organic Hole Conductor. *J. Phys. Chem. Lett.* **2010**, *1*, 1524. [CrossRef]
7. Patrick, C.E.; Giustino, F. Structural and Electronic Properties of Semiconductor-Sensitized Solar-Cell Interfaces. *Adv. Funct. Mater.* **2011**, *21*, 4663. [CrossRef]
8. Zhou, Y.; Wang, L.; Chen, S.; Qin, S.; Liu, X.; Chen, J.; Xue, D.; Luo, M.; Cao, Y.; Cheng, Y.; et al. Thin-film Sb_2Se_3 photovoltaics with oriented one-dimensional ribbons and benign grain boundaries. *Nat. Photonics* **2015**, *9*, 409. [CrossRef]
9. Wang, L.; Li, D.; Li, K.; Chen, C.; Deng, H.X.; Gao, L.; Zhao, Y.; Jiang, F.; Li, L.; Huang, F.; et al. Stable 6%-efficient Sb_2Se_3 solar cells with a ZnO buffer layer. *Nat. Energy* **2017**, *2*, 17046. [CrossRef]
10. Rabin, O.; Perez, J.; Grimm, J.; Wojtkiewicz, G.; Weissleder, R. An X-ray computed tomography imaging agent based on long-circulating bismuth sulphide nanoparticles. *Nat. Mater.* **2006**, *5*, 118. [CrossRef]
11. Yao, K.; Zhang, Z.; Liang, X.; Chen, Q.; Peng, L.M.; Yu, Y. Effect of H_2 on the Electrical Transport Properties of Single Bi_2S_3 Nanowires. *J. Phys. Chem. B* **2006**, *110*, 21408. [CrossRef] [PubMed]
12. Cademartiri, L.; Scotognella, F.; O'Brien, P.; Lotsch, B.; Thomson, J.; Petrov, S.; Kherani, N.; Ozin, G. Cross-Linking Bi_2S_3 Ultrathin Nanowires: A Platform for Nanostructure Formation and Biomolecule Detection. *Nano Lett.* **2009**, *9*, 1482. [CrossRef] [PubMed]
13. A review on properties, applications, and deposition techniques of antimony selenide. *Sol. Energy Mater. Sol. Cells* **2021**, *230*, 111223. [CrossRef]
14. Chen, S.; Liu, T.; Zheng, Z.; Ishaq, M.; Liang, G.; Fan, P.; Chen, T.; Tang, J. Recent progress and perspectives on Sb_2Se_3-based photocathodes for solar hydrogen production via photoelectrochemical water splitting. *J. Energy Chem.* **2022**, *67*, 508. [CrossRef]
15. Li, Q.; Zhang, W.; Peng, J.; Yu, D.; Liang, Z.; Zhang, W.; Wu, J.; Wang, G.; Li, H.; Huang, S. Nanodot-in-Nanofiber Structured Carbon-Confined Sb_2Se_3 Crystallites for Fast and Durable Sodium Storage. *Adv. Funct. Mater.* **2022**, *32*, 2112776. [CrossRef]
16. Ma, X.; Chen, W.; Tong, L.; Liu, S.; Dai, W.; Ye, S.; Zheng, Z.; Wang, Y.; Zhou, Y.; Zhang, W.; et al. Experimental demonstration of harmonic mode-locking in Sb_2Se_3-based thulium-doped fiber laser. *Opt. Laser Technol.* **2021**, *143*, 107286. [CrossRef]
17. Zhu, L.; Wang, H.; Wang, Y.; Lv, J.; Yanmei, M.; Cui, Q.; Ma, Y.; Zou, G. Substitutional Alloy of Bi and Te at High Pressure. *Phys. Rev. Lett.* **2011**, *106*, 145501. [CrossRef]
18. Einaga, M.; Ohmura, A.; Nakayama, A.; Ishikawa, F.; Yamada, Y.; Nakano, S. Pressure-induced phase transition of Bi_2Te_3 to a bcc structure. *Phys. Rev. B* **2011**, *83*, 092102. [CrossRef]
19. Zhao, J.; Liu, H.; Ehm, L.; Chen, Z.; Sinogeikin, S.; Zhao, Y.; Gu, G. Pressure-Induced Disordered Substitution Alloy in Sb_2Te_3. *Inor. Chem.* **2011**, *50*, 11291. [CrossRef]
20. Vilaplana, R.; Santamaría-Pérez, D.; Gomis, O.; Manjón, F.J.; González, J.; Segura, A.; Muñoz, A.; Rodríguez-Hernández, P.; Pérez-González, E.; Marín-Borrás, V.; et al. Structural and vibrational study of Bi_2Se_3 under high pressure. *Phys. Rev. B* **2011**, *84*, 184110. [CrossRef]
21. Ma, Y.; Liu, G.; Zhu, P.; Wang, H.; Wang, X.; Cui, Q.; Liu, J.; Ma, Y. Determinations of the high-pressure crystal structures of Sb_2Te_3. *J. Phys. Condens. Matter* **2012**, *24*, 475403. [CrossRef]
22. Liu, G.; Zhu, L.; Yanmei, M.; Lin, C.; Liu, J.; Ma, Y. Stabilization of 9/10-Fold Structure in Bismuth Selenide at High Pressures. *J. Phys. Chem. C* **2013**, *117*, 10045. [CrossRef]
23. Zhao, J.; Liu, H.; Ehm, L.; Dong, D.; Chen, Z.; Gu, G. High-pressure phase transitions, amorphization, and crystallization behaviors in Bi_2Se_3. *J. Phys. Condens. Matter* **2013**, *25*, 125602. [CrossRef] [PubMed]
24. Yu, Z.; Wang, L.; Hu, Q.; Zhao, J.; Yan, S.; Yang, K.; Sinogeikin, S.; Gu, G.; Mao, H.K. Structural phase transitions in Bi_2Se_3 under high pressure. *Sci. Rep.* **2015**, *5*, 15939. [CrossRef]
25. Hao, X.; Zhu, H.; Guo, Z.; Li, H.; Gong, Y.; Chen, D. Local insight to the structural phase transition sequence of Bi_2Se_3 under quasi-hydrostatic and nonhydrostatic pressure. *J. Phys. Condens. Matter* **2021**, *33*, 215402. [CrossRef]
26. Tseng, Y.C.; Lin, C.M.; Jian, S.R.; Le, P.H.; Gospodinov, M.M.; Marinova, V.; Dimitrov, D.Z.; Luo, C.W.; Wu, K.H.; Zhang, D.Z.; et al. Structural and electronic phase transition in $Bi_2Se_{2.1}Te_{0.9}$ under pressure. *J. Phys. Chem. Solids* **2021**, *156*, 110123. [CrossRef]
60. Ovsyannikov, S.V.; Shchennikov, V.V. High-Pressure Routes in the Thermoelectricity or How One Can Improve a Performance of Thermoelectrics. *Chem. Mater.* **2010**, *22*, 635. [CrossRef]
60. Ovsyannikov, S.V.; Shchennikov, V.V.; Vorontsov, G.V.; Manakov, A.Y.; Likhacheva, A.Y.; Kulbachinskii, V.A. Giant improvement of thermoelectric power factor of Bi_2Te_3 under pressure. *J. App. Phys.* **2008**, *104*, 053713. [CrossRef]
29. Zhang, J.L.; Zhang, S.J.; Weng, H.M.; Zhang, W.; Yang, L.X.; Liu, Q.Q.; Feng, S.M.; Wang, X.C.; Yu, R.C.; Cao, L.Z.; et al. Pressure-induced superconductivity in topological parent compound Bi_2Te_3. *Proc. Natl. Acad. Sci. USA* **2011**, *108*, 24. [CrossRef]
30. Zhang, C.; Sun, L.; Chen, Z.; Zhou, X.; Wu, Q.; Yi, W.; Guo, J.; Dong, X.; Zhao, Z. Phase diagram of a pressure-induced superconducting state and its relation to the Hall coefficient of Bi_2Te_3 single crystals. *Phys. Rev. B* **2011**, *83*, 140504. [CrossRef]
31. Zhu, J.; Kong, P.P.; Zhang, S.J.; Yu, X.H.; Zhu, J.L.; Liu, Q.Q.; Li, X.; Yu, R.C.; Ahuja, R.; Yang, W.G.; et al. Superconductivity in Topological Insulator Sb_2Te_3 Induced by Pressure. *Sci. Rep.* **2013**, *3*, 2016. [CrossRef] [PubMed]
32. Kong, P.P.; Zhang, J.L.; Zhang, S.J.; Zhu, J.; Liu, Q.Q.; Yu, R.C.; Fang, Z.; Jin, C.Q.; Yang, W.G.; Yu, X.H.; et al. Superconductivity of the topological insulator Bi_2Se_3 at high pressure. *J. Phys. Condens. Matter* **2013**, *25*, 362204. [CrossRef]
33. Taguchi, T.; Ikeda, M.; Li, H.; Suzuki, A.; Yang, X.; Ishii, H.; Liao, Y.F.; Ota, H.; Goto, H.; Eguchi, R.; et al. Superconductivity of topological insulator $Sb_2Te_{3-y}Se_y$ under pressure. *J. Phys. Condens. Matter* **2021**, *33*, 485704. [CrossRef] [PubMed]

34. Crichton, W.A.; Bernal, F.L.M.; Guignard, J.; Hanfland, M.; Margadonna, S. Observation of the Sb_2S_3-type post-post-$GdFeO_3$-perovskite: A model structure for high density ABX_3 and A_2X_3 phases. *arXiv* **2014**, arXiv:1410.2783.
35. Crichton, W.A.; Bernal, F.L.; Guignard, J.; Hanfland, M.; Margadonna, S. Observation of Sb_2S_3-type post-post-perovskite in $NaFeF_3$. Implications for ABX_3 and A_2X_3 systems at ultrahigh pressure. *Mineral. Mag.* **2016**, *80*, 659. [CrossRef]
36. Efthimiopoulos, I.; Zhang, J.; Kucway, M.; Park, C.; Ewing, R.; Wang, Y. Sb_2Se_3 under pressure. *Sci. Rep.* **2013**, *3*, 2665. [CrossRef] [PubMed]
37. Efthimiopoulos, I.; Kemichick, J.; Zhou, X.; Khare, S.; Ikuta, D.; Wang, Y. High-pressure Studies of Bi_2S_3. *J. Phys. Chem. A* **2014**, *118*, 1713. [CrossRef]
38. Sorb, Y.A.; Rajaji, V.; Malavi, P.S.; Subbarao, U.; Halappa, P.; Peter, S.C.; Karmakar, S.; Narayana, C. Pressure-induced electronic topological transition in Sb_2S_3. *J. Phys. Condens. Matter* **2015**, *28*, 015602. [CrossRef] [PubMed]
39. Ibañez, J.; Sans, J.A.; Popescu, C.; López-Vidrier, J.; Elvira-Betanzos, J.J.; Cuenca-Gotor, V.P.; Gomis, O.; Manjón, F.J.; Rodríguez-Hernández, P.; Muñoz, A. Structural, Vibrational, and Electronic Study of Sb_2S_3 at High Pressure. *J. Phys. Chem. C* **2016**, *120*, 10547. [CrossRef]
40. Li, C.; Zhao, J.; Hu, Q.; Liu, Z.; Yu, Z.; Yan, H. Crystal structure and transporting properties of Bi_2S_3 under high pressure: Experimental and theoretical studies. *J. Alloys Compd.* **2016**, *688*, 329. [CrossRef]
41. Cheng, H.; Zhang, J.; Yu, P.; Gu, C.; Ren, X.; Lin, C.; Li, X.; Zhao, Y.; Wang, S.; Li, Y. Enhanced Structural Stability of Sb_2Se_3 via Pressure-Induced Alloying and Amorphization. *J. Phys. Chem. C* **2020**, *124*, 3421. [CrossRef]
60. Anversa, J.; Chakraborty, S.; Piquini, P.; Ahuja, R. High pressure driven superconducting critical temperature tuning in Sb_2Se_3 topological insulator. *Appl. Phys. Lett.* **2016**, *108*, 212601. [CrossRef]
43. Kong, P.; Sun, F.; Xing, L.; Zhu, J.; Zhang, S.; Li, W.; Wang, X.; Feng, S.; Yu, X.; Zhu, J.; et al. Superconductivity in Strong Spin Orbital Coupling Compound Sb_2Se_3. *Sci. Rep.* **2014**, *4*, 6679. [CrossRef] [PubMed]
44. Das, S.; Sirohi, A.; Kumar Gupta, G.; Kamboj, S.; Vasdev, A.; Gayen, S.; Guptasarma, P.; Das, T.; Sheet, G. Discovery of highly spin-polarized conducting surface states in the strong spin-orbit coupling semiconductor Sb_2Se_3. *Phys. Rev. B* **2018**, *97*, 235306. [CrossRef]
45. Zhang, K.; Xu, M.; Li, N.; Xu, M.; Zhang, Q.; Greenberg, E.; Prakapenka, V.B.; Chen, Y.S.; Wuttig, M.; Mao, H.K.; et al. Superconducting Phase Induced by a Local Structure Transition in Amorphous Sb_2Se_3 under High Pressure. *Phys. Rev. Lett.* **2021**, *127*, 127002. [CrossRef]
46. Cheng, Y.; Cojocaru-Mirédin, O.; Keutgen, J.; Yu, Y.; Küpers, M.; Schumacher, M.; Golub, P.; Raty, J.Y.; Dronskowski, R.; Wuttig, M. Understanding the Structure and Properties of Sesqui-Chalcogenides (i.e., V_2VI_3 or Pn_2Ch_3 (Pn = Pnictogen, Ch = Chalcogen) Compounds) from a Bonding Perspective. *Adv. Mater.* **2019**, *31*, 1904316. [CrossRef]
47. Efthimiopoulos, I.; Buchan, C.; Wang, Y. Structural properties of Sb_2S_3 under pressure: Evidence of an electronic topological transition. *Sci. Rep.* **2016**, *6*, 24246. [CrossRef]
48. Dai, L.; Liu, K.; Li, H.; Wu, L.; Hu, H.; Zhuang, Y.; Linfei, Y.; Pu, C.; Liu, P. Pressure-induced irreversible metallization accompanying the phase transitions in Sb_2S_3. *Phys. Rev. B* **2018**, *97*, 024103. [CrossRef]
49. Wang, Y.; Yanmei, M.; Liu, G.; Wang, J.; Li, Y.; Li, Q.; Zhang, J.; Ma, Y.; Zou, G. Experimental Observation of the High Pressure Induced Substitutional Solid Solution and Phase Transformation in Sb_2S_3. *Sci. Rep.* **2018**, *8*, 14795. [CrossRef]
50. Liu, G.; Yu, Z.; Liu, H.; Redfern, S.A.T.; Feng, X.; Li, X.; Yuan, Y.; Yang, K.; Hirao, N.; Kawaguchi, S.I.; et al. Unexpected Semimetallic BiS_2 at High Pressure and High Temperature. *J. Phys. Chem. Lett.* **2018**, *9*, 5785. [CrossRef]
51. da Silva, E.L.; Skelton, J.M.; Rodríguez-Hernández, P.; Muñoz, A.; Santos, M.C.; Martínez-García, D.; Vilaplana, R.; Manjón, F.J. A theoretical study of the Pnma and R-3m phases of Sb_2S_3, Bi_2S_3 and Sb_2Se_3. *J. Mater. Chem. C* **2022**, *10*, 15061. [CrossRef]
52. Hohenberg, P.; Kohn, W. Inhomogeneous electron gas. *Phys. Rev.* **1964**, *136*, B864. [CrossRef]
53. Kresse, G.; Furthmüller, J. Efficiency of ab-initio total energy calculations for metals and semiconductors using a plane-wave basis set. *Comput. Mater. Sci.* **1996**, *6*, 15. [CrossRef]
54. Perdew, J.P.; Ruzsinszky, A.; Csonka, G.I.; Vydrov, O.A.; Scuseria, G.E.; Constantin, L.A.; Zhou, X.; Burke, K. Restoring the density-gradient expansion for exchange in solids and surfaces. *Phys. Rev. Lett.* **2008**, *100*, 136406; Erratum in *Phys. Rev. Lett.* **2009**, *102*, 039902. [CrossRef] [PubMed]
55. Monkhorst, H.J.; Pack, J.D. Special Points for Brillouin-Zone Integrations. *Phys. Rev. B* **1976**, *13*, 5188. . PhysRevB.13.5188. [CrossRef]
56. Murnaghan, F.D. The Compressibility of Media under Extreme Pressures. *Proc. Natl. Acad. Sci. USA* **1944**, *30*, 244. [CrossRef]
57. Birch, F. Finite Elastic Strain of Cubic Crystals. *Phys. Rev.* **1947**, *71*, 809. [CrossRef]
58. Togo, A.; Oba, F.; Tanaka, I. First-principles calculations of the ferroelastic transition between rutile-type and $CaCl_2$-type SiO_2 at high pressures. *Phys. Rev. B* **2008**, *78*, 134106. [CrossRef]
60. Gonzalez, J.M.; Nguyen-Cong, K.; Steele, B.A.; Oleynik, I.I. Novel phases and superconductivity of tin sulfide compounds. *J. Chem. Phys* **2018**, *148*, 194701. [CrossRef]
60. Nguyen, L.T.; Makov, G. GeS Phases from First-Principles: Structure Prediction, Optical Properties, and Phase Transitions upon Compression. *Cryst. Growth Des.* **2022**, *22*, 4956. [CrossRef]
61. Xu, M.; Jakobs, S.; Mazzarello, R.; Cho, J.Y.; Yang, Z.; Hollermann, H.; Shang, D.; Miao, X.; Yu, Z.; Wang, L.; et al. Impact of Pressure on the Resonant Bonding in Chalcogenides. *J. Phys. Chem. C* **2017**, *121*, 25447. [CrossRef]

62. Cuenca-Gotor, V.P.; Sans, J.A.; Gomis, O.; Mujica, A.; Radescu, S.; Muñoz, A.; Rodríguez-Hernández, P.; da Silva, E.L.; Popescu, C.; Ibañez, J.; et al. Orpiment under compression: Metavalent bonding at high pressure. *Phys. Chem. Chem. Phys.* **2020**, *22*, 3352. [CrossRef] [PubMed]
63. Grimme, S. Semiempirical GGA-Type Density Functional Constructed with a Long-Range Dispersion Correction. *J. Comp. Chem.* **2006**, *27*, 1787. [CrossRef] [PubMed]
64. Perdew, J.P.; Zunger, A. Self-interaction correction to density-functional approximations for many-electron systems. *Phys. Rev. B* **1981**, *23*, 5048. [CrossRef]
65. Born, M. On the stability of crystal lattices. I. In *Mathematical Proceedings of the Cambridge Philosophical Society*; Cambridge University Press: Cambridge, UK, 1940; Volume 36, p. 160. [CrossRef]
66. Dove, M.T. *Introduction to Lattice Dynamics*; Cambridge University Press: Cambridge, UK, 1993. [CrossRef]
67. Dove, M.T. *Structure and Dynamics: An Atomic View of Materials*; Oxford Master Series in Physics; Oxford University Press: Oxford, UK, 2003. [CrossRef]
68. Dove, M.T. Review: Theory of displacive phase transitions in minerals. *Am. Min.* **2015**, *82*, 213. [CrossRef]
69. Venkataraman, G. Soft modes and structural phase transitions. *Bull. Mater. Sci.* **1979**, *1*, 129. [CrossRef]
70. Di Gennaro, M.; Saha, S.; Verstraete, M. Role of Dynamical Instability in the Ab Initio Phase Diagram of Calcium. *Phys. Rev. Lett.* **2013**, *111*, 025503. [CrossRef]
71. Quadbeck-Seeger, H.J. *World of the Elements: Elements of the World*; Wiley-VCH: Weinheim, Germany, 2007. [CrossRef]
72. Skelton, J.M.; Burton, L.A.; Parker, S.C.; Walsh, A.; Kim, C.E.; Soon, A.; Buckeridge, J.; Sokol, A.A.; Catlow, C.R.A.; Togo, A.; et al. Anharmonicity in the High-Temperature *Cmcm* Phase of SnSe: Soft Modes and Three-Phonon Interactions. *Phys. Rev. Lett.* **2016**, *117*, 075502. [CrossRef]
73. Skelton, J.M. ModeMap. Available online: https://github.com/JMSkelton/ModeMap (accessed on 10 June 2019).